A Neural Network Approach for Waveform Generation and Selection with Multi-Mission Radar

A Neural Network Approach for Waveform Generation and Selection with Multi-Mission Radar

James M. Kurdzo and John Y. N. Cho
Lincoln Laboratory
Massachusetts Institute of Technology
Lexington, MA, USA
James.Kurdzo@ll.mit.edu
jync@ll.mit.edu

Boon Leng Cheong and Robert D. Palmer
Advanced Radar Research Center
University of Oklahoma
Norman, OK, USA
boonleng@ou.edu
rpalmer@ou.edu

***Abstract*—Nonlinear frequency modulated (NLFM) pulse compression waveforms have become a mainstream methodology for radars across multiple sectors and missions, including weather observation, target tracking, and target detection. NLFM affords the ability to generate a low-sidelobe autocorrelation function and matched filter while avoiding aggressive amplitude modulation, resulting in more power incident on the target. This capability can lead to significantly lower system design costs due to the possibility of sensitivity gains on the order of 3 dB or more compared with traditional, amplitude-modulated linear frequency modulated (LFM) waveforms. Generation of an optimal NLFM waveform, however, can be an arduous task, and may involve complex optimization and non-closed-form solutions. For a multi-mission or cognitive radar, which may utilize a wide combination of frequencies, pulse lengths, and amplitude modulations (among other factors), this could lead to an extremely large waveform table for selection. This paper takes a neural network approach to this problem by optimizing a set of over 100 waveforms spanning a wide space and using the results to interpolate the waveform possibilities to a higher resolution. A modified form of a previous NLFM method is combined with a four-hidden-layer neural network to show the integrated and peak range sidelobes of the generated waveforms across the model training space. The results are applicable to multi-mission and cognitive radars that need precise waveform specifications in rapid succession. The expected waveform generation times are addressed and quantified, and the potential applicability to multi-mission and cognitive radars is discussed.**

***Index Terms*—radar, weather, waveform design, pulse compression, optimization, neural networks, machine learning, nonlinear frequency modulation**

I. Introduction

The advent of nonlinear frequency modulated (NLFM) pulse compression waveforms in multiple classes of radar has introduced a capability for decreasing range sidelobes while maintaining high sensitivity through the use of limited (or no) amplitude modulation [1], [2]. Recent advances in this area have been particularly highlighted in the weather radar realm, due to the necessity of low peak and integrated sidelobes for the accurate detection and representation of distributed targets [3]–[9]. While these solutions may be acceptable for a single-use-case scenario, there are difficulties that arise in multi-function and cognitive radars [10]–[13]. The methodology in [7], for example, involves a complex optimization process with a non-closed-form solution, making it a time-consuming process to develop a waveform for one set of chirp bandwidth, pulse length, amplitude modulation, etc. Multi-mission and cognitive radars of the future would conceivably need a large set of waveform parameter combinations, resulting in the potential for extremely large waveform tables. For example, if a hypothetical radar was expected to have waveforms to fit every combination of chirp bandwidths from 1-100 MHz at 0.1-MHz resolution, pulse widths from 10-200 μs at 1-μs resolution, and amplitude modulation from 0.5 (unitless) to 1 at 0.01 resolution, this would result in a waveform table with nearly 10 million combinations. At approximately 5 hours per optimization, and using 10,000 consecutive cores on a supercomputing grid, it could take nearly 7 months to design the waveform table.

This is important because multi-mission radars may need to pick waveforms "on the fly" to minimize spectral interference or track a target with sufficient resolution. These combinations of parameters could be exceptionally specific, requiring many different waveforms to be available. It is also important to note that cognitive radars have been hypothesized to be able to change waveforms from pulse to pulse [10], [11], necessitating the selection of appropriate waveforms on extremely short timescales (on the order of milliseconds). The focus of this paper is the capability for extremely rapid generation of radar waveforms for a multi-mission or cognitive radar using a neural network approach. This technique utilizes a modified form of the NLFM method described in [7] to optimize over 100 individual waveforms. These waveforms are fed to a four-hidden-layer neural network that outputs expected Bézier parameters that define the frequency chirp for candidate waveforms in approximately 10 ms. This approach effectively acts as an interpolation method for the waveform input parameters and the associated Bézier output parameters, eliminating the need to optimize millions of separate waveforms. The resolution of this interpolation is theoretically infinite in the model training space, allowing the radar to choose extremely specific waveform parameter combinations.

DISTRIBUTION STATEMENT A. Approved for public release. Distribution is unlimited. This material is based upon work supported by the Federal Aviation Administration under Air Force Contract No. FA8702-15-D-0001. Any opinions, findings, conclusions or recommendations expressed in this material are those of the author(s) and do not necessarily reflect the views of the Federal Aviation Administration.

978-1-7281-1679-2/19/$31.00 ©2019 IEEE

Multiple organizations are exploring the future use of multi-mission and rapid-scanning radars, including the Federal Aviation Administration (FAA) and the National Weather Service (NWS) [12]–[14]. The Airport Surveillance Radar 9 (ASR-9) is an example of a multi-mission radar, as it provides both tracking and weather capabilities at sites with an on-board Weather Systems Processor (WSP). In a future ASR-9/WSP replacement, for example, the radar could be scanning a gust front impinging on an airfield at moderate temporal and spatial resolution (as part of an FAA weather mission) in one part of its domain and observing a non-cooperative target at high temporal and spatial resolution in another part of its domain. Low-reflectivity targets such as gust fronts and the desire to obtain clear-air data via Bragg scatter are strong drivers for pulse compression for weather-related missions. The gust front mission would require a long pulse for sensitivity but reduced bandwidth due to the lack of need for extremely high spatial resolution. The non-cooperative target may allow for a shorter pulse if it is a highly reflective target and/or is close to the radar (i.e., within the blind range of a longer pulse), but might require a very high bandwidth in order to determine the type of target with high certainty. Not only are different waveforms necessary on the fly for the radar completing these two missions, but neighboring radars would have to adapt to the large bandwidth of the primary radar, possibly with the need to complete other missions with fewer spectral resources. This dynamic environment describes the need for very large waveform tables or "on-the-fly" methods.

Although the results of the neural network waveforms in this study are not quite on par with the individually optimized waveforms, it is suspected that this technique can be refined and improved in the future. This paper shows promise for the technique, not a final result. This paper also serendipitously shows improvements to the NLFM methodology in [7], with nearly direct comparisons to the previous method that demonstrate improved results.

II. Methodology

A. Modifications to NLFM Technique

In [7], the fitness function that determines optimization performance is based on peak sidelobe level and null-to-null mainlobe width. The weakness of this approach is raised in [9], which cites the advantage of focusing on integrated sidelobe level for distributed targets. The fitness function from [7] was therefore modified to take the form of:

$$F = \frac{ISL}{MLW} \tag{1}$$

where ISL is integrated sidelobe level (in dB) and MLW is the null-to-null mainlobe width (in m). The fitness, F, is targeted for minimization. Note that ISL will always be a negative value, resulting in the objective of lowering the ISL and minimizing the MLW. In addition to this change to the fitness function, the updated method adds a 3-dB range resolution target (which joins the null-to-null mainlobe width target in [7]). This parameter allows for a wider 3-dB mainlobe width than would be typically expected for a given bandwidth, allowing for some of the resulting energy to be used in minimizing sidelobes. Both the 3-dB and null-to-null mainlobe width targets act as hard stops for the associated parameters, meaning that the optimization is deemed infeasible if the parameter exceeds the target. These parameters are typically represented by scaling factors relative to the expected 3-dB mainlobe width (i.e., the relation between the speed of light, c, and the bandwidth, B). For this study, scaling factors of 2 and 10 were used for the 3-dB range resolution and the null-to-null mainlobe width, respectively. For example, a chirp bandwidth of 5 MHz would result in an expected 3-dB mainlobe width of 30 m, and scaling factors of 2 and 10 would target mainlobe widths of 60 m and 300 m at 3 dB and null-to-null, respectively.

Finally, changes for the Bézier pull vector limits were made. Previously, there were user-defined limits to these vectors, which was due to the goal of minimizing the search space for faster convergence on a solution. For this study, the limits were expanded and normalized to the specifications fed into the optimization. The pull vectors, which define the search grid in the optimization, were changed to -1.5 to +1.5 in the bandwidth dimension (where the chirp bandwidth is normalized between -1 and +1 about the center frequency, with the edges akin to half the bandwidth). In the pulse length dimension, the range is from -0.125 to +0.5 (where the pulse length is normalized between 0 and 1). The search space is defined by the sampling frequency and a scaled divisor that define a grid of possible Bézier pull vector locations. For the examples shown in this study, a sampling frequency of 160 MHz was used, and a divisor of 1,000 was used in the bandwidth dimension. This leads to 3,001 possible bandwidth-dimension pull vector destinations and, for example, 24,001 possible time-dimension pull vector destinations for a 100-μs pulse length, resulting in a grid of over 72 million points. With 6 pull vectors and two dimensions each, the search space becomes approximately 1.94 x 10^{94} possible combinations. This is approximately 10^{57} times the search space than that reported in [7].

B. Neural Network Design

The NLFM design technique utilized in this study can take at least 5 hours to complete, depending on how confident the user desires the algorithm to be at termination. The neural network approach is necessary because a full waveform table for a multi-mission or cognitive radar would take prohibitively too long to develop, especially when considering complications related to transmitter droop and distortion. The number of hidden layers was varied between 1 and 15, and a training/validation/test ratio of 70/15/15 was used. A shallow, fully connected, feed-forward regression neural network was trained for each hidden layer size, and the results were subjectively analyzed in order to determine an appropriate hidden layer size. A Levenberg-Marquardt backpropogation optimization was used. For this study, 4 hidden layers were used in the neural network due to the performance evident relative to

978-1-7281-1679-2/19/$31.00 ©2019 IEEE

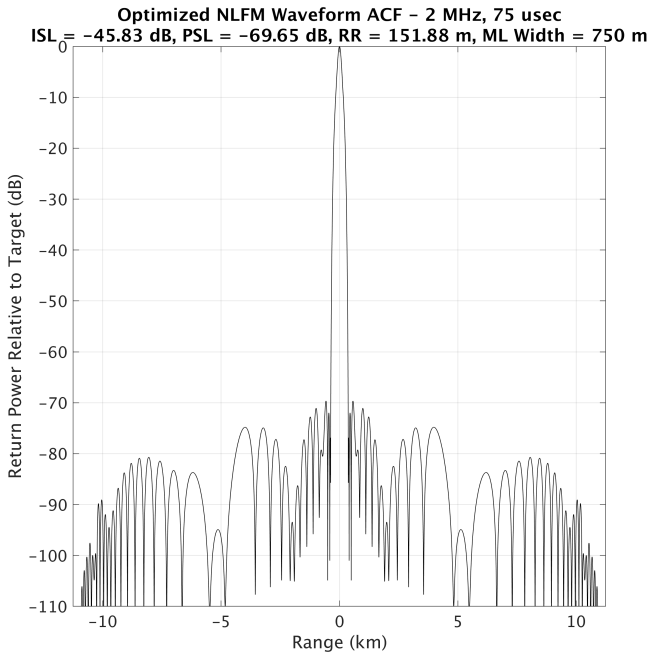

Fig. 1. Autocorrelation function (ACF) for an optimized NLFM waveform with a 2-MHz chirp bandwidth, a 75-μs pulse length, and a 0.1 roll-off factor raised-cosine amplitude taper. The observed ISL is -45.83 dB, and the observed PSL is -69.65 dB. The 3-dB range resolution and null-to-null mainlobe width targets and results are relaxed compared to [7].

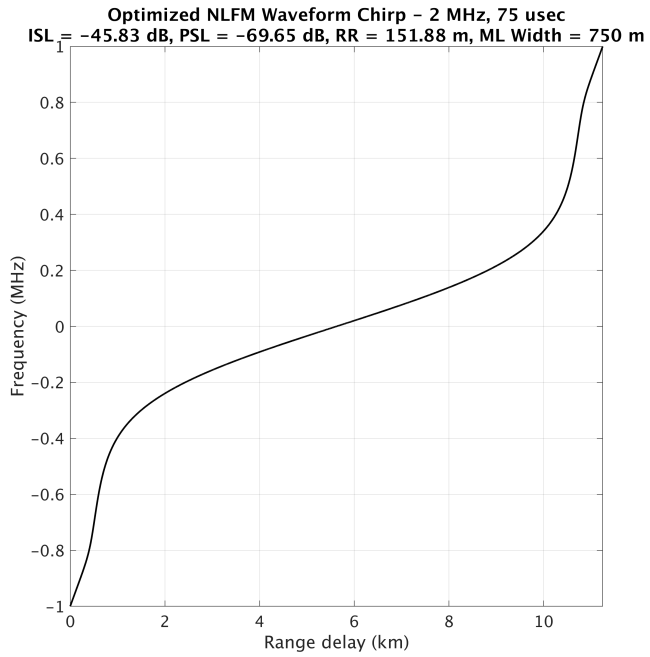

Fig. 2. Frequency chirp pattern for an optimized NLFM waveform with a 2-MHz chirp bandwidth, a 75-μs pulse length, and a 0.1 roll-off factor raised-cosine amplitude taper. This pattern corresponds to the autocorrelation function (ACF) shown in Fig. 1.

the other tested values. The inputs to the neural network are bandwidth and pulse length, while amplitude modulation, 3-db range resolution target, and null-to-null mainlobe width target were set at 0.1, 2, and 10, respectively. The amplitude modulation represents a 0.1 roll-off factor of a raised-cosine taper, leading to 0.24 dB of SNR loss relative to a rectangular pulse. The outputs are the 12 Bézier pull vector parameters. It is important to note that additional combinations of parameters (amplitude modulation, mainlobe widths, etc.) can be ingested into the neural network, assuming a sweep of these parameters is represented in the training data.

The series of pulse lengths used in the training data was 20, 25, 30, 35, 40, 45, 50, 60, 75, 100, 125, 150, 175, and 200 μs. The series of chirp bandwidths used was 0.5, 1, 2, 3, 4, 5, 7.5, and 10 MHz. This resulted in 112 optimized waveforms that were fed into training of the neural network. Each waveform had two input parameters (pulse length and bandwidth) and 12 outputs (the 12 Bézier parameters). It should be noted that this is an exceptionally small training dataset for a neural network. It is anticipated that a denser spacing of parameters (i.e., the optimization of more waveforms) would improve the results shown in this study due to less data sparsity. We recognize this challenge and limitation, but hope to expand our training dataset in the future.

III. Results

In order to offer a comparison to the results in [7], the true, optimized waveform that is closest to the 2.2-MHz, 67-μs (147.4 time-bandwidth product) example shown in [7] is analyzed here (i.e., part of the training dataset). This waveform is a 2-MHz chirp with a 75-μs pulse length (150 time-bandwidth product), and its autocorrelation function is shown in Fig. 1. A one-to-one comparison with [7] is not possible due to the spacing of the training dataset. The new waveform displays ISL of -45.83 dB and PSL of -69.65 dB, compared with ISL of -37 dB and PSL of -59 dB in [7]. The 3-dB range resolution and null-to-null mainlobe width have been relaxed, however, with values of 151.88 m and 750 m, respectively, compared to 120 m and 405 m in [7]. This yields a somewhat unfair comparison between the two waveforms, which must be kept in mind; this is due to the fact that more-relaxed parameters were allowed for the neural network approach. Note that the amplitude modulations are equal, with both using a raised-cosine taper with a roll-off factor of 0.1.

The chirp pattern for the optimized 150 time-bandwidth waveform is shown in Fig. 2. As with most NLFM waveforms that utilize light amplitude modulation, the chirp rate is slightly lower on the edges of the pulse where the taper takes effect. The chirp rate then increases before becoming relatively linear through the middle half of the pulse. This "rotated S" shape has been noted in the literature before [2] and is similar to that seen in [7]. As the amplitude modulation is increased, the slower chirp rate presses toward the middle of the pulse (not shown) due to the lack of energy available in the areas of lower power. As with many other examples in the literature, all of the NLFM waveforms used in this study are forced to

978-1-7281-1679-2/19/$31.00 ©2019 IEEE

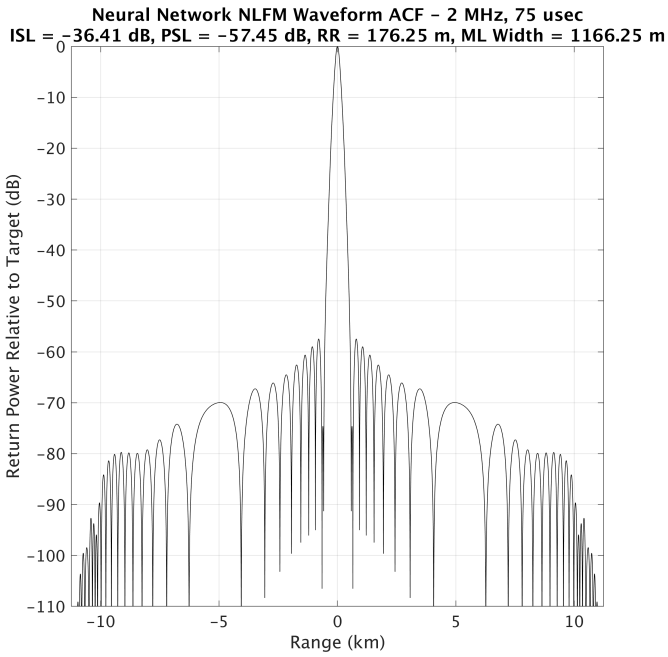

Fig. 3. Autocorrelation function (ACF) for a neural network-based NLFM waveform with a 2-MHz chirp bandwidth, a 75-μs pulse length, and a 0.1 roll-off factor raised-cosine amplitude taper. The observed ISL is -36.41 dB, and the observed PSL is -57.45 dB. The 3-dB range resolution and null-to-null mainlobe width are degraded compared to the example in Fig. 1.

be symmetric due to the enhanced Doppler tolerance noted in [15]. Although Doppler tolerance is not shown in this paper, it is similar in nature to Fig. 6 in [7]. PSL, in general, raises approximately 10-15 dB at 25 m s^{-1} Doppler shift, and approximately 20 dB at 50 m s^{-1} Doppler shift.

Waveform specifications, such as the example shown in Figs. 1 and 2, and the resulting Bézier parameters were given as input to the neural network with the goal of generating new waveforms rapidly. This would allow for an effective interpolation of the waveform table in a multi-function or cognitive radar, vastly increasing the table size. The most viable method for comparing the model's capabilities is to compare the optimized waveform from Figs. 1 and 2 with the model output for the same waveform specifications. The model output (i.e., test data) for a 2-MHz, 75-μs waveform (for direct comparsion with Figs. 1 and 2) is shown in Fig. 3. The ISL is -36.41 dB, while the PSL is -57.45 dB. This is a significantly degraded waveform compared to the optimized version, but it should be noted that the results are similar in nature to those in [7] with the non-modified NLFM method. With that said, as with the optimized version, the 3-dB range resolution and null-to-null mainlobe width are significantly widened, somewhat limiting the usefulness of the model's waveform. However, this method is still in an experimental stage, and the ability for the model to generate a viable waveform is promising.

Although the performance is degraded, a critical detail for the modeled waveform is that it was generated in approximately 10 ms. This is compared with the roughly 24 hours it took to fully optimize the waveform in Figs. 1 and 2. When the time to generate a waveform is considered, the waveform performance should be weighed against this variable. For a multi-function or cognitive radar, the ability to generate waveforms on the fly is critical to the radar's functionality. With a larger training dataset and more parameter dimensions in the model, we hope to improve the functionality for even better results that can be generated in the same amount of time.

Finally, the performance of the neural network should be quantified across the spectrum of the possible design space. This type of analysis gives a clear indication of the model's ability to serve its function, which is to act as an interpolator across the parameter dimensions. Waveforms were generated with bandwidths spanning 1.5 MHz to 10 MHz at 0.25-MHz resolution, and pulse lengths spanning 25 μs to 200 μs at 1-μs resolution. This analysis generates 6,688 waveforms in just over a minute, compared with the 112 optimized waveforms that took days to process. The resulting ISL and PSL values (from the test data) are shown in Figs. 4 and 5, respectively. As expected, as the time-bandwidth product increases, sidelobe levels generally decrease, especially in the ISL. ISL values range from -25 dB at relatively low time-bandwidth products, to -55 to -60 dB at time bandwidth products over 1,000. A pseudo pareto front of "acceptable" (arbitrarily) ISL values at or below -35 dB can be drawn from roughly 2 MHz and 50 μs to 4 MHz and 25 μs, or a time-bandwidth product of 100. Similar parameters tend to yield PSL values at or below -55 dB.

It should be noted that 3-dB range resolutions and null-to-null mainlobe widths are not shown, but they are generally higher than the optimized versions of the waveforms. This can be mitigated by building the scaling factors for these parameters into the model, something we have not yet been able to accomplish due to the higher computational complexity necessary. The resulting ISL and PSL values would likely degrade, but this is an ongoing area of research.

IV. Discussion

Effective and timely generation of waveforms is an important task for any multi-mission or cognitive radar. The neural network technique presented in this paper supports the generation of acceptable waveforms in an exceptionally short amount of time. Of particular note is the improvement to the existing NLFM method in [7] and how it allows for neural network-based waveform statistics to be similar to the results in [7]. The modified fitness function is much improved, but there is still ongoing work to perfect the technique. Without specifically including PSL in the fitness function, it is conceivable that higher sidelobes adjacent to the mainlobe will be observed in optimized waveforms. Additionally, there is less impetus to keep a thin mainlobe if attempting to minimize ISL, however this is somewhat mitigated by the existence of the MLW term in the denominator of the fitness function.

The optimization method is still in need of ideal parameters for the Bézier pull vector limits. This issue exists in

978-1-7281-1679-2/19/$31.00 ©2019 IEEE

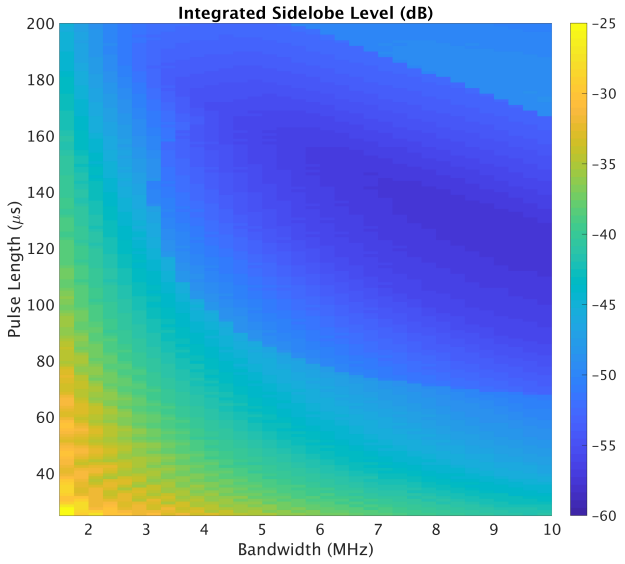

Fig. 4. Integrated sidelobe level (ISL) for a range of neural network waveforms ranging from 1.5 to 10 MHz and 25 to 200 μs. Each waveform was generated in approximately 10 ms, yielding 6,688 waveforms in just over a minute. Based on the results of [7], the ISL levels are comparable or better for most time-bandwidth products above 100.

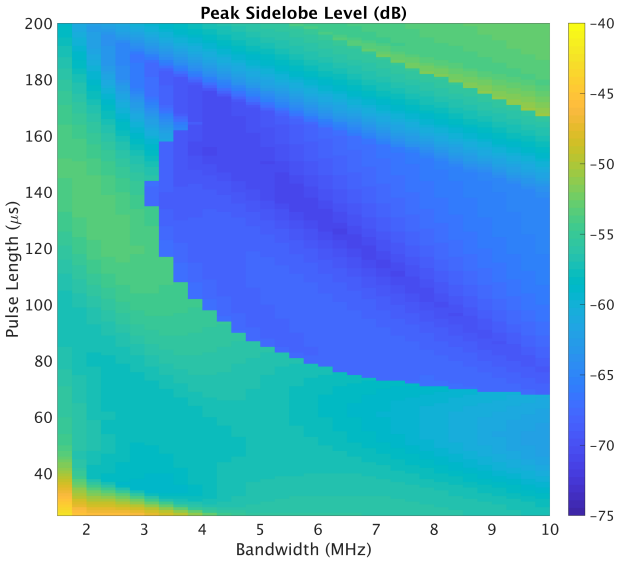

Fig. 5. Peak sidelobe level (PSL) for a range of neural network waveforms ranging from 1.5 to 10 MHz and 25 to 200 μs. Each waveform was generated in approximately 10 ms, yielding 6,688 waveforms in just over a minute. Based on the results of [7], the PSL levels are comparable or better for most time-bandwidth products above 100.

two opposite senses: first, it would be prudent to limit the search space for computational complexity reasons. Second, we would like to be able to generate the most "flexible" chirp functions possible. If the limits are too wide, the search space becomes too large and it is difficult to achieve convergence. Additionally, it can be difficult to get an optimal shape to the chirp function. If the limits are too narrow, it is unlikely that a near-global optimum will be found. It is particularly difficult to achieve the optimal Bézier pull vector limits at very low and very high time-bandwidth products. This work is ongoing, and as mentioned later in this section, will eventually be applied to the neural network approach.

The neural network results show degraded performance compared with the optimized waveforms, but may still be considered "acceptable" for certain missions. In addition to elevated sidelobes, the mainlobe width is generally about 50% larger than the optimized waveforms. This can be mitigated in two related ways: first, increase the number of mainlobe width scaling factors. For this study, only a factor of 10 was used. Smaller factors would force smaller mainlobe widths, but also likely result in higher sidelobes. Second, increasing the number of optimized waveforms fed to the neural network would vastly improve the model. For computational reasons, we were restricted to the 112 waveforms used in this study. Expanding dimensionalities, resolution, and range would improve the robustness of the model. Other methodologies could also be explored, such as a support vector regression model. It is not known if a shallow neural network is the best option for the goal of rapid waveform design.

As previously mentioned, the range of parameters should be increased in future iterations of this work. We only included bandwidths up to 10 MHz and pulse lengths of 25-200 μs. Certain applications will require significantly more bandwidth, or longer/shorter pulse lengths. These "edges" of waveform parameters are difficult to generalize due to the need to change the Bézier pull vector spatial limits and resolutions across time-bandwidth space. Work is ongoing to simplify this process and expand the reach of the NLFM method presented in this paper. It is expected that improved results at low and high time-bandwidth products will allow for an expansion of the neural network method in the near future. This expansion will also lead to a growth in the training dataset for the neural network, further aiding in the model's expected performance.

Finally, the speed of waveform generation can be expected to improve with time and using other design platforms, including advanced hardware such as Graphical Processing Units (GPUs). The waveforms in this study were designed with MATLAB, which is not the fastest-processing scripting language. An implementation either in a compiled language or on, for example, a field-programmable gate array (FPGA) would theoretically vastly improve the time it takes to generate the necessary waveform with the pre-trained model. Additionally, the ability for a radar to store recently used and commonly used waveforms would also decrease the time needed to generate a waveform. With the ability to generate waveforms on the order of ms, true pulse-to-pulse waveform selection

978-1-7281-1679-2/19/$31.00 ©2019 IEEE

is possible, and scan-to-scan selection is already feasible, as shown in this paper.

The impact of multi-mission and cognitive radars to future radar-based goals is expected to be significant [10], [12], [13]. Not only can multi-mission radars decrease overall network costs due to the ability to cover multiple needs, but the capabilities inherent in, for example, a phased-array or imaging radar [16], [17] could revolutionize the way we use radar for missions such as weather observation and air traffic control. Part of this concept, however, includes the possibility of optimizing the radar for each mission on the fly. Additionally, radio frequency spectrum is a large consideration for a multi-mission or cognitive radar network. Such radars would need to both fit into the existing spectral landscape and also fit into the spectral characteristics of the network they are a part of.

V. Conclusions

This paper presents a modified approach to NLFM waveform design that uses ISL and MLW in a fitness function for optimizing waveform parameters. Modifications to [7] include a new fitness function, a 3-dB range resolution restriction, and an increased search space size through the use of modified Bézier pull vector limits. A comparison to the results in [7] is presented in order to demonstrate the performance enhancements of the altered method. This method is applied to the optimization of 112 different waveforms spanning 20–200 μs in pulse length and 0.5–10 MHz in chirp bandwidth. Each of the optimized waveforms is used as input to a shallow neural network, with the pulse length and bandwidth serving as inputs, and the 12 Bézier parameters serving as outputs. The trained neural network model is then used to generate 6,688 waveforms in just over one minute (compared with the days it took to generate the original 112 waveforms). The results of the neural network-generated waveforms are presented over the model training space, showing an effective "interpolation" of the waveform parameters, and the ability to generate arbitrary waveforms on the order of 10 ms.

Future work will involve further modification of the fitness function and Bézier pull vector limits for the core optimization technique. This will allow for better waveform statistics at the "edges" of the design space (i.e., very low and very high time-bandwidth products). This work will allow for expansion of the neural network, leading to increased usability and performance. Additionally, we plan to increase the dimensionality of the model to include amplitude modulation, 3-dB range resolution limit, and null-to-null mainlobe width limit. We also would like to optimize waveforms at a higher effective "resolution" in the parameter space. These changes will vastly increase the training dataset size, leading to a more robust neural network. Finally, we plan to implement this methodology in a real-time system, allowing us to quantify realistic waveform generation times in a system-based framework. We also plan to use the University of Oklahoma's PX-1000 [18] and PX-10000 radars to test our new waveform methodology and implement on-the-fly distortion corrections for model-generated waveforms.

Acknowledgment

The authors would like to thank Guifu Zhang and John Meier for their assistance with the original waveform design technique described in this paper. Discussions with Mark Veillette and Chris Mattioli were helpful in the implementation of the shallow neural network.

References

[1] H. D. Griffiths and L. Vinagre, "Design of low-sidelobe pulse compression waveforms," *IEEE Electronics Letters*, vol. 30, no. 12, pp. 1004–1005, 1994.

[2] E. De Witte and H. D. Griffiths, "Improved ultra-low range sidelobe pulse compression waveform design," *IEEE Electronics Letters*, vol. 40, no. 22, pp. 1448–1450, 2004.

[3] R. J. Keeler and C. A. Hwang, "Pulse compression for weather radar," in *International Radar Conference*. Alexandria, VA: IEEE, 1995, pp. 529–535.

[4] A. S. Mudukutore, V. Chandrasekar, and R. J. Keeler, "Pulse compression for weather radars," *IEEE Trans. on Geoscience and Remote Sensing*, vol. 36, no. 1, pp. 125–142, 1998.

[5] F. O'Hora and J. Bech, "Improving weather radar observations using pulse-compression techniques," *Meteorol. Appl.*, vol. 14, no. 4, pp. 389–401, 2007.

[6] N. Bharadwaj and V. Chandrasekar, "Wideband waveform design principles for solid-state weather radars," *J. Atmos. Oceanic Technol.*, vol. 29, no. 1, pp. 14–31, 2012.

[7] J. M. Kurdzo, B. L. Cheong, R. D. Palmer, G. Zhang, and J. B. Meier, "A pulse compression waveform for improved-sensitivity weather radar observations," *J. Atmos. Oceanic Technol.*, vol. 31, no. 12, pp. 2713–2731, 2014.

[8] C. M. Nguyen and V. Chandrasekar, "Sensitivity enhancement system for pulse compression weather radar," *J. Atmos. Oceanic Technol.*, vol. 31, no. 12, pp. 2732–2748, 2014.

[9] S. M. Torres, C. D. Curtis, and D. Schvartzman, "Requirement-driven design of pulse compression waveforms for weather radars," *J. Atmos. Oceanic Technol.*, vol. 34, no. 6, pp. 1351–1369, 2017.

[10] S. Haykin, "Cognitive radar: A way of the future," *IEEE Signal Processing Magazine*, vol. 23, no. 1, pp. 30–40, 2006.

[11] S. Haykin, Y. Xue, and T. N. Davidson, "Optimal waveform design for cognitive radar," in *IEEE 42nd Asilomar Conference on Signals, Systems and Computers*, 2008.

[12] M. E. Weber, J. Y. N. Cho, J. S. Herd, J. M. Flavin, W. E. Benner, and G. S. Torok, "The next-generation multimission U.S. surveillance radar network," *Bull. Amer. Meteor. Soc.*, vol. 88, pp. 1739–1751, 2007.

[13] D. S. Zrnić, J. F. Kimpel, D. E. Forsyth, A. Shapiro, G. Crain, R. Ferek, J. Heimmer, W. Benner, T. J. McNellis, and R. J. Vogt, "Agile-beam phased array radar for weather observations," *Bull. Amer. Meteor. Soc.*, vol. 88, pp. 1753–1766, 2007.

[14] P. L. Heinselman, D. L. Priegnitz, K. L. Manross, T. M. Smith, and R. W. Adams, "Rapid sampling of severe storms by the national weather radar testbed phased array radar," *Wea. Forecasting*, vol. 23, no. 5, pp. 808–824, 2008.

[15] N. Levanon and E. Mozeson, *Radar Signals*. Wiley, 2004.

[16] B. Isom, R. Palmer, R. Kelley, J. Meier, D. Bodine, M. Yeary, B.-L. Cheong, Y. Zhang, T.-Y. Yu, and M. I. Biggerstaff, "The atmospheric imaging radar: Simultaneous volumetric observations using a phased array weather radar," *J. Atmos. Oceanic Technol.*, vol. 30, no. 4, pp. 655–675, 2013.

[17] J. M. Kurdzo, F. Nai, D. J. Bodine, T. A. Bonin, R. D. Palmer, B. L. Cheong, J. Lujan, A. Mahre, and A. D. Byrd, "Observations of severe local storms and tornadoes with the atmospheric imaging radar," *Bull. Amer. Meteor. Soc.*, vol. 98, no. 5, pp. 915–935, 2017.

[18] B. L. Cheong, R. Kelley, R. D. Palmer, Y. Zhang, M. Yeary, and T.-Y. Yu, "PX-1000: A solid-state polarimetric X-band weather radar and time-frequency multiplexed waveform for blind range mitigation," *IEEE Trans. on Instrumentation and Measurement*, vol. 62, no. 11, pp. 3064–3072, 2013.

978-1-7281-1679-2/19/$31.00 ©2019 IEEE